JOURNAL OF AGRICULTURAL AND FOOD CHEMISTRY

Article

pubs.acs.org/JAFC

Effect of High-Fat Diet on Hepatic Proteomics of Hamsters

Chen-Chung Liao,[†] Ya-Lin Lin,[‡] and Chia-Feng Kuo*[,‡]

[†]Proteomics Research Center, National Yang-Ming University, Taipei 112, Taiwan

[‡]Department of Food Science, Nutrition, and Nutraceutical Biotechnology, Shih Chien University, Taipei 104, Taiwan

Supporting Information

ABSTRACT: A high-fat diet contributes to the etiology of metabolic diseases. As the liver plays a crucial role in metabolism, an insight into the hepatic proteomics will help to illustrate the physiological effect of a high-fat diet. Fourteen nine-week old male Syrian hamsters were maintained on either control (C) or high-fat (HF) diets (0.2% cholesterol +22% fat) for 8 weeks. Hamsters were chosen because they show close similarity to human lipid metabolism. At the end of study, blood and livers were collected for analysis. Liver proteins were fractionated by electrophoresis, digested by trypsin, and then separated by label-free nano-LC/MS/MS. The TurboSequest algorithm was used to identify the peptide sequences against the hamster database in Universal Proteins Resource Knowledgebase (UniProt). The results indicate that 1191 hepatic proteins were identified and 135 of them were expressed differentially in the high-fat group ($p < 0.05$). Some of these 135 proteins that involve in metabolic diseases were further validated by Western blotting. The animals maintained on the high-fat diet had significantly ($p < 0.05$) higher serum triglyceride, cholesterol, aspartate aminotransferase (AST), alanine aminotransferase (ALT), and uric acid. Animals consuming a high-fat diet also had significantly ($p < 0.05$) more accumulation of triglyceride and cholesterol in livers. Xanthine dehydrogenase (XDH), which plays an important role in uric acid synthesis, was up-regulated by the high-fat diet ($p < 0.05$). The α-subunit of hydroxyacyl-CoA dehydrogenase/3-ketoacyl-CoA thiolase/enoyl-CoA hydratase (HADHA), which catalyzes the second and third reactions of β-oxidation, was down-regulated by the high-fat diet ($p < 0.05$). Aconitate hydratase 2 (ACO2), which catalyzes the conversion of citrate to isocitrate in TCA cycle, was down-regulated in animals of the high-fat group ($p < 0.05$). Inflammatory markers annexin A3 (ANXA3) and annexin A5 (ANXA5) were up-regulated by the high-fat diet ($p < 0.05$). Moreover, enzymes involved in the urea cycle were suppressed by high-fat diet, including carbamoyl phosphate synthase 1 (CPS1), ornithine transcarbamoylase (OTC), argininosuccinate synthase (ASS), argininosuccinate lyase (ASL), and arginase 1 (ARG 1). Post-translational modifications (PTM) of ANXA3, ANXA5, and XDH were also analyzed. A set of differentially expressed proteins were identified as molecular markers for elucidating the pathological mechanism of high-fat diet.

KEYWORDS: *high-fat diet, hamster, liver, proteomics, post-translational modification*

INTRODUCTION

Chronic consumption of a high-fat diet predisposes subjects to body weight gain with development of metabolic syndrome, as manifested by obesity, hyperlipidemia, and insulin resistance. Individuals with metabolic syndrome are at a higher risk of cardiovascular disease, type II diabetes mellitus, and non-alcoholic fatty liver diseases (NAFLD).[1] NAFLD is composed of a spectrum of clinical abnormalities ranging from fatty liver only (excessive accumulation of lipids) to nonalcoholic steatohepatitis (NASH) and cirrhosis in the absence of alcohol abuse.[2] NAFLD is the leading cause of chronic liver injury in the nonalcoholic population. Although some clinical abnormalities are reversible, NAFLD may progress to more severe stages including hepatocarcinoma if not diagnosed early and treated properly.[3]

Disruption of the normal synthesis, transport, and removal of triglycerides (TG) is the basis for abnormal accumulation of lipids within the liver. An increased dietary supply of fat promotes the growth of adipose tissue. As the mass of adipose tissue is enlarging, the release of TNF-α from adipose tissue increases. TNF-α activates IκB kinase β (IκκB), inhibiting phosphorylaiton of insulin receptor substrates (IRS-1 and IRS-2) and up-regulating hepatic fatty acid translocase, which in turn leads to increased release of long-chain fatty acid (LCFA) into circulation and enhanced uptake by liver.[4,5] Conversion of LCFA to TG by glycerol phosphate acyltranferase is not rate-limiting in hepatocytes; therefore, increased availability of LCFAs will lead to increased TG synthesis and accumulation.[6] An increased dietary supply of fat also promotes weight gain and the development of obesity. Elevated plasma insulin level in overweight individuals up-regulates hepatic *de novo* synthesis of TG through sterol regulatory element-binding protein-1c (SREBP-1c) and carbohydrate response element-binding protein (ChREBP).[7]

A high-fat diet contributes to the etiology of metabolic diseases. As liver plays a crucial role in metabolism, an insight into the hepatic proteomics of animals will help to illustrate the physiological effect of a high-fat diet. Proteomics is a large-scale comprehensive study of proteins, including information on protein abundances and modification along with their interacting networks.[8] Proteomic analysis is a powerful tool in studying the changes in protein expression and identification of biomarkers for pathogenic processes.[9−11] Many mass-spec-

Received: October 27, 2014
Revised: January 27, 2015
Accepted: January 29, 2015
Published: January 29, 2015

DOI: 10.1021/jf506118j
J. Agric. Food Chem. 2015, 63, 1869−1881

trometry (MS)-based proteomic techniques have been developed. Among them, two-dimensional electrophoresis (2-DE) and label-free liquid chromatography (LC)-MS/MS shotgun analysis are mostly applied.[12] In 2-DE, separated proteins are detected by staining and isolated from the gel, followed by matrix-assisted laser desorption/ionization mass spectrometry (MALDI-MS) or surface-enhanced laser desorption/ionization mass spectrometry (SELDI-MS).[13] Shotgun proteomics performs the mass spectrometry in data-dependent acquisition mode. In this mode, peptide fragmentation is guided by the abundance of detectable precursor ions. The specific detected peptide ions are further selected for collision induced dissociation (CID) and fragment ion (MS2) spectra. The recorded information is then searched against protein sequence database to deduce the peptide sequences and corresponding proteins.[14] Compared with 2-DE, shotgun proteomics shows higher sensitivity, protein throughput, quantitative accuracy, proteome coverage, and reproducibility.[15]

Although several studies have been performed to investigate the effect of high-fat diet on hepatic proteomics, rats or mice were chosen instead of hamsters.[16−19] Hamsters are considered a better model for the study of metabolic diseases because they respond consistently to dietary modulation and show close similarity to the human lipoprotein profile compared to other rodents.[20] The aim of this study was to explore the differences in hepatic protein expression between hamsters fed control diet and high-fat diet by shotgun proteomic analysis. We hypothesized that a set of differentially expressed proteins will be identified as molecular markers for elucidating the pathological mechanism of high-fat diet.

MATERIALS AND METHODS

Antibodies. Antiaconitate hydratase, antixanthine dehydrogenase, and antiannexin 5 were purchase from Epitomics (Burlingame, CA). Antiadenosine kinase was obtained from Novus (Littleton, CO). Anti-HADHA (trifunctional enzyme subunit α, mitochondria) and antiannexin 3 were purchased from Proteintech Group (Chicago, IL). Goat antirabbit peroxidase-conjugated antibody was purchased from Jackson ImmunoResearch (West Grove, PA).

Animals and Diets. Male eight-week-old Syrian hamsters purchased from National Laboratory Animal Breeding and Research Center (Taipei, Taiwan) were maintained at 22 ± 2 °C and 12-h light/dark cycle. After 1 week of acclimation, animals were randomly assigned to the control group or the high-fat diet group (n = 7). The diets and water were provided *ad libitum*. Feed intake and body weights were measured daily and once a week, respectively. The ingredients of the control diet are (g/kg) corn starch, 452; sucrose, 200; casein, 200; soybean oil, 50; AIN-76 mineral mix, 35; AIN-76 vitamin mix, 10; methylated cellulose, 50; DL-methionine, 3. In the high-fat diet, 170 g of lard and 2 g of cholesterol per kilogram were supplemented to replace part of the corn starch. At the end of 8 weeks, all animals were sacrificed. Bloods and livers were collected for biochemical and proteomic analysis (Supporting Information Figure 1). This protocol was approved by Shih Chien University Animal Care and Use Committee.

Determination of Serum Lipids, Uric Acid, AST, and ALT. Serum TG, total cholesterol (TC), and HDL-cholesterol (HDL-C) were determined by using commercial kits (Fortree Diagnostics, Antrim, U.K.). Serum uric acid (UA), aspartate aminotransferase (AST), and alanine aminotransferase (ALT) were also quantified by the kits (Randox, Antrim, U.K.).

Determination of Liver Lipids. Liver lipids were measured according to the method of Folch et al. with modification.[21] In brief, the livers were homogenized with Folch reagent (chloroform/methanol = 2:1, v/v) at the ratio of 20:1. The homogenates were centrifuged at 936g for 10 min. Equal volumes of supernatant and triton-100 (Sigma, St. Louis, MO) were mixed and left in the fume hood to remove organic solvent before the contents of lipids were measured by commercial kits (Randox, Antrim, U.K.).

Liver Histoloty. Liver tissues were fixed in 10% buffered formalin overnight, embedded in paraffin, sectioned at 5 μm thickness, and stained with hematoxylin and eosin (H&E). The slides were examined with histopathological findings recorded by a veterinary pathologist who was blinded to the treatments.

SDS-PAGE and In-Gel Digestion. Total proteins of each sample (50 μg) were fractionated by SDS-PAGE (dodecyl sulfate polyacrylamide gel electrophoresis), and the gel was stained with Coomassie Brilliant Blue G-250 (Bio-Rad, Hercules, CA). The proteins in each lane were separated and sliced into 10 fractions based on molecular weight, followed by destaining in a solution of 25 mM NH_4HCO_3 and 50% (v/v) acetonitrile (1:1). After drying in a Speed-Vac (Thermo Election, Waltham, MA), all the gel slices were incubated with 25 mM NH_4HCO_3 and 1% β-mercaptoethanol in the dark for 20 min to reduce the disulfide bonds, followed by the incubation with solution consists of 5% 4-vinylpyridine in 25 mM NH_4HCO_3 and 50% acetonitrile (1:1) for 20 min for alkylation of the cysteine residues. Subsequently, the slices were dried in the Speed-Vac for 20 min. The in-gel digestion by the action of modified trypsin (Promega, Mannheim, Germany) in 25 mM NH_4HCO_3 (1%, w/v) was performed at 37 °C overnight. The digested peptides were removed from the gel, washed by 25 mM NH_4HCO_3 for 10 min, dried by Speed-Vac, and then kept at −20 °C until further analysis. The peptides were resuspended in 0.1% formic acid immediately prior to subsequent analysis.[22]

Mass Spectrometric Analysis. The tryptic peptides were analyzed by a nanoflow high-performance liquid chromatography system (Agilent Technologies 1200 series, Waldbronn, Germany) coupled to an LTQ-Orbitrap Discovery hybrid mass spectrometer with a nanoelectrospray ionization source (Thermo Electron, Waltham, MA). An analytical column (100 × 0.075 mm, 3.5 μm, Angilent C18) was operated at a flow rate of 0.5 μL/min in conjunction with a gradient elution solvent system using solvent A (0.1% formic acid in water) and solvent B (0.1% formic acid in acetonitrile). The course of gradient elution was programmed as a 30 min linear gradient of 5% to 35% solvent followed by 95% solvent B for a duration of 10 min. After each full scan at the m/z range 200−2000, a data-dependent acquired MS/MS scan for precursor ions was selected on the basis of conventional MS spectra performed at high resolution (M/DM, 60000 full width half-maximum). From each spectrum, the precise mass value and the charge state of the precursor ions were obtained. Following MS_1, the fragment ions were generated on the basic of collision-induced dissociation (CID) spectrum.[23]

Database Search. The spectra generated from nano-LC/MS/MS were analyzed by Xcalibur 2.0 SRI software (Thermo Electron, Waltham, MA). The TurboSequest algorithm was used to identify the peptide sequences against the hamster database in Universal Proteins Resource knowledgebase (UniProt; http://www.unipro.org/).[24] The peptides were filtered by Xcorr versus charge state with a significance level of 0.05. Xcorr was used for a match with 1.9 for singly charged ions, 2.2 for doubly charged ions, and 3.75 for triply charged ions. The proteins were identified as hepatic proteins when more than two peptides from a single protein met the Xcorr score. The mass spectra of candidate biomarkers were analyzed by our in-house post-translational modification (PTM) finder programs PTM-Miner and PTM-Q for identification of PTM peptide sequence, site of PTM, and quantification. Fix modification on the cysteine residues (carboxyamidomethylation, 57 Da), variable modification on the methionine residues (methionine, 16 Da), fragment mass tolerance at 1 Da, and peptide mass tolerance at 1.5 Da were not considered as specific PTM. The fragmented ions obtained were labeled as b, y, y-NH_3, and b-H_2O ions.[22,25]

Ingenuity Pathways Analysis. Accession numbers of proteins expressed differently in high-fat group were uploaded as an Excel file into the Ingenuity Pathway Analysis (IPA) software (http://www.igenuity.com). The proteins were grouped by known relationships into "functional analysis" and "canonical pathway analysis" of a network.

DOI: 10.1021/jf506118j
J. Agric. Food Chem. 2015, 63, 1869−1881

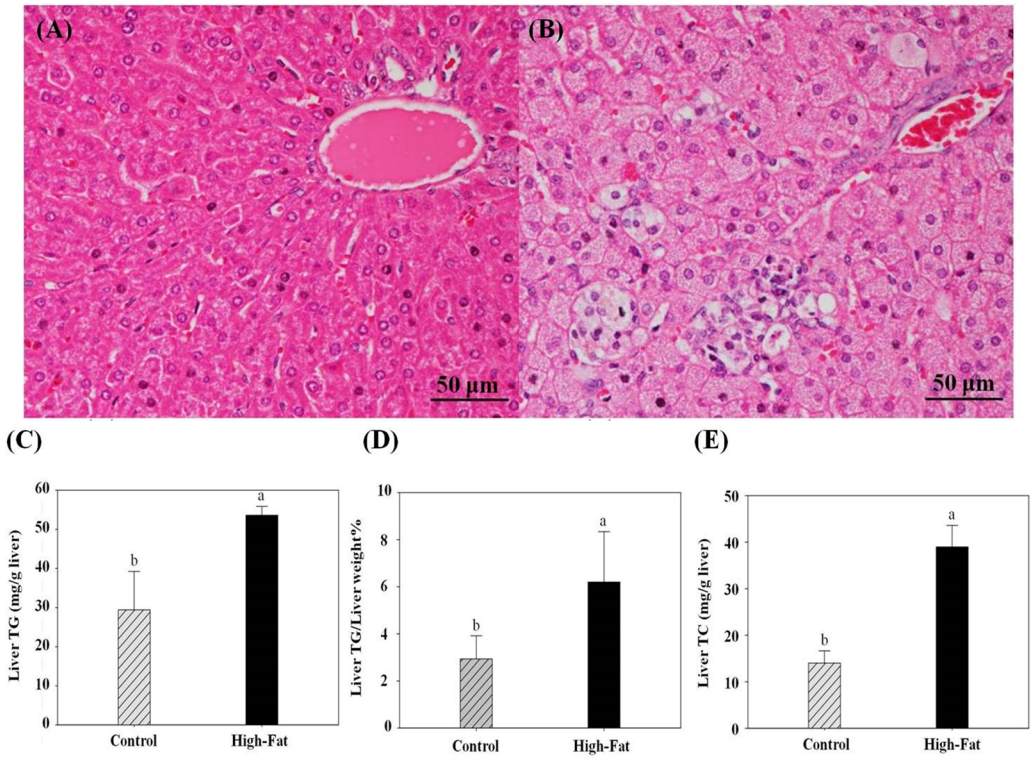

Figure 1. H&E stain of liver tissues from (A) control and (B) high-fat groups (400×). Panels C, D, and E show liver TG, relative weight of TG in liver (%), and liver TC, respectively. Hamsters were sacrificed after 8 weeks of feeding on the control diet or the high-fat diet. TG, triglyceride; TC, total cholesterol. Groups with the same letter are not significantly different (α = 0.05).

The significance of association between proteins and functional/canonical pathways was computed by Fisher's exact text (α = 0.05). IPA calculates a *p*-score as $-\log_{10}(p\text{-value})$ to rank networks. A score of 3 or higher indicates that the proteins are not clustered in a pathway by random chance at the confidence level of 99.99% or higher.[21,26]

Western Blotting. Livers were thawed on ice and homogenized in 25 mM Tris-HCl, pH 7.5, containing 250 mM sucrose and 1 mM ethylene-diaminetetra-acetic acid (10%, w/v). The homogenate was centrifuged at 105 000*g* for 30 min. After centrifugation, the supernatant was collected for analysis and its protein content was determined by Dc Protein Assay Kit (Bio-Rad, Hercules, CA). An equal amount of proteins from each sample was separated by SDS-PAGE before being transferred to polyvinylidene fluoride (PVDF) membranes (PerkinElmer, Waltham, MA). The membranes were blocked with 5% nonfat dry milk in Tris-buffered saline containing Tween (TBST) (20 mM Tris-HCl, pH 8.3, 137 mM NaCl, and 0.1% Tween-20) for 1 h before being sequentially incubated with primary antibody overnight in a cold room and horseradish peroxidase-conjugated secondary antibody for 1 h at room temperature. Immunoreactive proteins were detected using an enhanced chem-iluminescence kit (ECL, PerkinElmer, Waltham, MA), and the film was analyzed by ImageQuant software (Molecular Dynamics, Sunnyvale, CA). For stripping and reprobing, the membrane was incubated with stripping buffer (0.2 M glycine, 3.5 mM SDS, 0.1% Tween-20, pH 2.2) at room temperature for 10 min. After the buffer was discarded, the membrane was incubated with fresh stripping buffer for another 10 min followed by two 10 min washes by PBS buffer and two 5 min washes by TBST buffer. After striping, the blocking and probing were performed as mentioned above.[22]

Statistical Analysis. Statistical analysis was performed using the Statistical Analysis System (SAS Institute, Cary, NC). The *t*-test was used to determine significant difference among control group and high-fat group (α = 0.05).

RESULTS AND DISCUSSION

Hepatic proteomics is an important parameter for the studies of metabolic diseases. The animal model and the diet both have significant influences on the results of proteomic analysis. In most of the hepatic proteomic studies, rats or mice were chosen as models.[16−19] However, hamsters that show closer similarity to human lipid metabolism compared to rats/mice were used as the model in this present study. Hamsters and other rodents respond differently to dietary fats. Similar to humans, hamsters were hyper-responsive to the dietary cholesterol whereas rats were hypo-responsive.[27] Moreover, the effect of dietary cholesterol on lipoprotein profile in hamsters is similar to that of humans.[28] It is clear that hamsters could be a better model to study the physiological effect of dietary fats.

In addition to the difference in animal model, the composition of diet in current study is different from those in other proteomic studies. In this study, 17% lard and 0.2% cholesterol were supplemented to the diet (42.27% of calories from fats) to induce hyperlipidemia and accumulation of lipids in liver. In Zhang et al.'s proteomic study, 60% fructose was used to induce fatty liver in hamsters.[29] In a rat proteomic study, 2% cholesterol, 7% lard, and 10% yolk powder were used to formula a high-fat diet.[16] Luo et al. used a commercial 60% fat diet to study changes in hepatic protein abundance in mice.[18] Baiges et al. used bacon, sweets, biscuits with foie gras, cheese, muffins, carrots, and milk with sugar to formulate a cafeteria high-fat diet.[17] Different diet formulas lead to different results in proteomic analysis. The diet of this current study closely lines up with the Western pattern diet, which typically contains high amounts of saturated fat and sugar.

In our present study, we used label-free nano-LC/MS/MS (shotgun proteomics), a high-throughput proteomic tool, to

DOI: 10.1021/jf506118j
J. Agric. Food Chem. 2015, 63, 1869−1881

Table 1. Proteins Expressed Differentially in the High-Fat Group

	protein name	protein ID	control (mean ± SE)	HF[a] (mean ± SE)	fold[b]	t-test p-value[c]
1	14−3−3 protein γ	G3HA25	0 ± 0	2.32 ± 0.69	100	0.0156
2	14−3−3 protein γ	G3IPD7	0 ± 0	1.23 ± 0.44	100	0.0310
3	annexin A3	G3IEB1	0 ± 0	2.25 ± 0.59	100	0.0084
4	elongation factor 1-β	G3HDL6	0 ± 0	1.1 ± 0.39	100	0.0296
5	endoplasmic reticulum resident protein 29	G3H284	0 ± 0	1.05 ± 0.42	100	0.0465
6	fibrinogen A-α-chain (fragment)	Q08283	0 ± 0	0.69 ± 0.23	100	0.0247
7	histone H1.5-like protein	A0A061IB71	0 ± 0	1.12 ± 0.38	100	0.0270
8	selenium-binding protein 1	G3H302	0 ± 0	0.68 ± 0.23	100	0.0249
9	succinyl-CoA ligase [GDP-forming] subunit β, mitochondrial	G3GS40	0 ± 0	1.68 ± 0.58	100	0.0272
10	titin	G3HAC6	0 ± 0	1.29 ± 0.29	100	0.0046
11	valyl-tRNA synthetase	G3HZE9	0 ± 0	1.03 ± 0.37	100	0.0309
12	annexin	A0A061IML2	0.18 ± 0.18	2.58 ± 0.38	14.58	0.0012
13	annexin A5	G3I5A4	0.18 ± 0.18	2.58 ± 0.38	14.58	0.0012
14	40S ribosomal protein S3a	G3HKG8	0.24 ± 0.24	2.9 ± 1.01	12.22	0.0428
15	3-hydroxyanthranilate 3,4-dioxygenase	G3GV35	0.35 ± 0.2	1.75 ± 0.51	4.93	0.0446
16	glutamine synthetase	G3HG36	1.19 ± 0.4	5.5 ± 1.21	4.63	0.0147
17	epoxide hydrolase 1	G3I0X4	0.61 ± 0.36	2 ± 0.27	3.27	0.0215
18	xanthine dehydrogenase/oxidase	G3I4G1	0.47 ± 0.27	1.52 ± 0.23	3.21	0.0264
19	xanthine dehydrogenase/oxidase-like protein	A0A061HWK7	0.47 ± 0.27	1.52 ± 0.23	3.21	0.0264
20	xanthine dehydrogenase/oxidase-like protein	A0A061I0 × 3	0.47 ± 0.27	1.52 ± 0.23	3.21	0.02648
21	xanthine dehydrogenase/oxidase-like protein	A0A061I342	0.47 ± 0.27	1.52 ± 0.23	3.21	0.02648
22	calnexin	Q920L9	0.37 ± 0.21	1.04 ± 0.09	2.83	0.0274
23	F-actin-capping protein subunit β-like protein	A0A061IH36	0.55 ± 0.18	1.34 ± 0.15	2.46	0.0152
24	F-actin-capping protein subunit β-like protein	A0A061II46	0.55 ± 0.18	1.34 ± 0.15	2.46	0.0152
25	major vault protein	A0A061IB55	5.08 ± 0.59	10.04 ± 1.52	1.98	0.0228
26	major vault protein	G3I4I9	5.08 ± 0.59	10.04 ± 1.52	1.98	0.0228
27	thiomorpholine-carboxylate dehydrogenase	A0A061IGJ9	2.63 ± 0.25	4.77 ± 0.65	1.82	0.0220
28	α-actinin-1	G3H1K9	3.33 ± 0.67	5.91 ± 0.46	1.78	0.0194
29	alanine−tRNA ligase, cytoplasmic	Q8CFX8	3.06 ± 0.26	5.22 ± 0.41	1.7	0.0042
30	adenylate kinase 2, mitochondrial	G3IPK9	1.98 ± 0.21	3.2 ± 0.32	1.62	0.0185
31	endoplasmin	G3HQM6	7.51 ± 0.94	12.01 ± 1.57	1.6	0.0490
32	adenylate kinase 2, mitochondrial	G3H928	3.82 ± 0.45	5.96 ± 0.69	1.56	0.0414
33	glutathione S-transferase	P70686	24.1 ± 1.66	36.63 ± 2.78	1.52	0.0082
34	aldehyde dehydrogenase, mitochondrial	P81178	13.2 ± 0.56	11.28 ± 0.15	−1.17	0.0163
35	carbamoyl-phosphate synthase [ammonia], mitochondrial	G3H4W9	143.45 ± 2.59	106.09 ± 8.47	−1.35	0.0055
36	aspartate aminotransferase	A0A061IAK8	7.59 ± 0.72	5.6 ± 0.23	−1.36	0.0395
37	apoptosis-inducing factor 1	A0A061HYH9	3.63 ± 0.46	2.21 ± 0.27	−1.64	0.0369
38	apoptosis-inducing factor 1	A0A061HZ30	3.63 ± 0.46	2.21 ± 0.27	−1.64	0.0369
39	apoptosis-inducing factor 1	G3H3X1	3.63 ± 0.46	2.21 ± 0.27	−1.64	0.0369
40	trifunctional enzyme subunit α, mitochondrial	G3GXQ3	11.24 ± 1.06	6.48 ± 0.68	−1.73	0.0092
41	stress-70 protein, mitochondrial	O35501	7.45 ± 0.79	4.17 ± 0.31	−1.79	0.0085
42	acetyl-CoA acetyltransferase, cytosolic	G3HGP4	4.24 ± 0.4	2.3 ± 0.17	−1.84	0.0040
43	sarcosine dehydrogenase, mitochondrial	G3IG06	4.6 ± 0.69	2.49 ± 0.29	−1.85	0.0304
44	fatty acid synthase	G3GXD7	33.26 ± 3.94	17.39 ± 2.47	−1.91	0.0142
45	aconitate hydratase, mitochondrial	G3II47	5.85 ± 0.64	3.04 ± 0.79	−1.92	0.0323
46	short/branched chain specific acyl-CoA dehydrogenase, mitochondrial	G3I5V3	3.64 ± 0.43	1.79 ± 0.45	−2.03	0.0249
47	plectin (fragment)	Q9JI55	20.74 ± 3.93	9.83 ± 1.81	−2.11	0.0452
48	ubiquitin	G3I129	17.11 ± 0.98	7.86 ± 1.46	−2.18	0.0019
49	arginase	E7CXR7	10.35 ± 1.16	4.57 ± 1.06	−2.27	0.0104
50	ubiquitin	G3GVL0	16.99 ± 0.64	7.42 ± 1.16	−2.29	0.0003
51	ornithine carbamoyltransferase, mitochondrial (fragment)	G3GSF7	2.76 ± 0.25	1.19 ± 0.03	−2.32	0.0007
52	polyubiquitin	P62976	62.31 ± 2.47	26.18 ± 4.25	−2.38	0.0003
53	cytochrome P450 2D27	Q9QYG6	1.53 ± 0.15	0.63 ± 0.21	−2.41	0.0141
54	3-hydroxyhexobarbital dehydrogenase 1/3-α, 17-β-hydroxysteroid dehydrogenase	Q8K4V1	2.68 ± 0.48	1.11 ± 0.38	−2.43	0.0420
55	transketolase	G3GUU5	6.02 ± 0.58	2.46 ± 0.46	−2.45	0.0029
56	ubiquitin/ribosomal protein CEP52 fusion protein	Q792I7	8.86 ± 0.32	3.5 ± 0.83	−2.53	0.0009
57	polyubiquitin	O35080	62.48 ± 2.28	24.11 ± 4.37	−2.59	0.0002
58	methylmalonyl-CoA mutase	A0A061ILK7	6.01 ± 0.54	2.24 ± 0.58	−2.68	0.0030
59	methylmalonyl-CoA mutase, mitochondrial	G3I6B2	6.01 ± 0.54	2.24 ± 0.58	−2.68	0.0030

DOI: 10.1021/jf506118j
J. Agric. Food Chem. 2015, 63, 1869−1881

Table 1. continued

	protein name	protein ID	control (mean ± SE)	HF[a] (mean ± SE)	fold[b]	t-test p-value[c]
60	abhydrolase domain-containing protein 14B	G3H894	2.03 ± 0.13	0.75 ± 0.44	−2.72	0.0317
61	tubulin β-2C chain	G3IG44	4.88 ± 0.56	1.69 ± 0.32	−2.88	0.0025
62	succinyl-CoA ligase [GDP-forming] subunit α, mitochondrial	G3HQ05	3.45 ± 0.23	1.17 ± 0.48	−2.96	0.0051
63	cytochrome P450 2D20	Q9QYG5	5.59 ± 0.32	1.86 ± 1.05	−3.01	0.0144
64	argininosuccinate lyase	G3IDU6	2.47 ± 0.32	0.82 ± 0.47	−3.01	0.0284
65	argininosuccinate lyase isoform 1	A0A061I991	2.47 ± 0.32	0.82 ± 0.47	−3.01	0.0284
66	acidic leucine-rich nuclear phosphoprotein 32 family member A	G3H8Q4	1.73 ± 0.28	0.54 ± 0.31	−3.22	0.0299
67	3 β-hydroxysteroid dehydrogenase/δ 5→4-isomerase type 2	Q64421	1.96 ± 0.38	0.6 ± 0.35	−3.26	0.0393
68	arginase	A0A061IMD3	3.36 ± 0.4	0.97 ± 0.36	−3.46	0.0042
69	peptidyl-prolyl *cis*−*trans* isomerase	G3H533	2.58 ± 0.19	0.72 ± 0.72	−3.56	0.0477
70	argininosuccinate synthase	G3IMU3	2.4 ± 0.28	0.65 ± 0.42	−3.7	0.0130
71	glyceraldehyde-3-phosphate dehydrogenase	G3GZ97	4 ± 0.33	1.08 ± 1.08	−3.72	0.0406
72	phosphatidylethanolamine-binding protein 1	G3GU60	3.27 ± 0.2	0.87 ± 0.87	−3.76	0.0358
73	histone H2A	G3HDT6	4.19 ± 0.38	1.04 ± 0.75	−4.01	0.00958
74	histone H3	G3H2T7	6.26 ± 0.76	1.49 ± 1.25	−4.2	0.0173
75	histone H2A type 1	G3HPV6	7.02 ± 0.75	1.66 ± 1.66	−4.22	0.0262
76	glutathione peroxidase	G3H8G0	4.17 ± 0.29	0.94 ± 0.94	−4.43	0.0168
77	aspartate aminotransferase	G3GZZ0	1.65 ± 0.13	0.37 ± 0.37	−4.44	0.0177
78	vacuolar protein sorting-associated protein 35	A0A061IC10	0.99 ± 0.12	0.22 ± 0.22	−4.56	0.0202
79	ATP synthase subunit δ (fragment)	A0A061IBF1	1.04 ± 0.05	0.22 ± 0.22	−4.81	0.0098
80	histone H4	G3HPV7	6.28 ± 0.53	1.3 ± 1.3	−4.83	0.0122
81	dynamin-like 120 kDa protein, mitochondrial	G3HWY6	1.05 ± 0.17	0.22 ± 0.22	−4.86	0.0237
82	nucleophosmin	G3IBF1	1.18 ± 0.29	0.23 ± 0.23	−5.1	0.0441
83	T-complex protein 1 subunit β	G3HZ42	1.27 ± 0.24	0.25 ± 0.25	−5.12	0.0256
84	ATP synthase subunit d, mitochondrial	G3GTF9	1.59 ± 0.3	0.29 ± 0.29	−5.5	0.0212
85	adenosine kinase	P55262	1.28 ± 0.17	0.23 ± 0.23	−5.56	0.0106
86	adenosine kinase	G3GWQ3	1.28 ± 0.17	0.23 ± 0.23	−5.56	0.0106
87	hemoglobin subunit α	P01945	24.46 ± 2.77	4.28 ± 3.8	−5.72	0.0051
88	histone H3.1t	G3HHM2	8.87 ± 1.2	1.45 ± 1.45	−6.13	0.0075
89	cytochrome b5	P70116	3.62 ± 0.26	0.58 ± 0.58	−6.26	0.0030
90	α-1,4 glucan phosphorylase	G3H6Z4	1.36 ± 0.3	0.22 ± 0.22	−6.27	0.0222
91	40S ribosomal protein SA	G3HQX0	1.47 ± 0.29	0.23 ± 0.23	−6.37	0.0152
92	phosphoenolpyruvate carboxykinase, cytosolic [GTP]	G3HBK8	1.61 ± 0.18	0.25 ± 0.25	−6.45	0.0043
93	peptidyl-prolyl *cis*−*trans* isomerase A	P14851	5.91 ± 0.18	0.87 ± 0.87	−6.81	0.0012
94	histone H2A	G3HDS3	5.09 ± 0.85	0.72 ± 0.72	−7.03	0.0079
95	amine oxidase [flavin-containing] B	G3I526	1.37 ± 0.28	0.19 ± 0.19	−7.3	0.0123
96	UDP-glucuronosyltransferase 1−7C	G3IET7	1.41 ± 0.19	0.19 ± 0.19	−7.53	0.0038
97	3 β-hydroxysteroid dehydrogenase type 3	O35296	0.96 ± 0.37	0 ± 0	−100	0.0413
98	3-hydroxyisobutyryl-CoA hydrolase, mitochondrial	G3IHA0	1.03 ± 0.35	0 ± 0	−100	0.0262
99	40S ribosomal protein S11	G3I004	1.06 ± 0.21	0 ± 0	−100	0.0022
100	40S ribosomal protein S14	P62265	2.2 ± 0.25	0 ± 0	−100	0.0001
101	40S ribosomal protein S17	P63274	1.41 ± 0.25	0 ± 0	−100	0.0012
102	aldo-keto reductase family 1 member C13	P82809	1.27 ± 0.43	0 ± 0	−100	0.0254
103	ankyrin-1 (fragment)	G3HHI1	1.26 ± 0.49	0 ± 0	−100	0.0406
104	ATP-dependent RNA helicase DDX3X	A0A061HXV1	0.79 ± 0.27	0 ± 0	−100	0.0257
105	ATP-dependent RNA helicase DDX3X	A0A061HYF2	0.79 ± 0.27	0 ± 0	−100	0.0257
106	cytochrome *b*-c1 complex subunit 9	G3HP15	0.67 ± 0.23	0 ± 0	−100	0.0256
107	cytochrome P-450	Q9QZ50	2.03 ± 0.3	0 ± 0	−100	0.0005
108	cytochrome P450 2C25	Q08078	1.52 ± 0.46	0 ± 0	−100	0.0157
109	cytochrome P450 2C27	P33264	1.71 ± 0.24	0 ± 0	−100	0.0003
110	cytochrome P450 2D20	G3I0E9	2.98 ± 1.01	0 ± 0	−100	0.0256
111	dihydropyrimidinase	G3HVF7	0.87 ± 0.29	0 ± 0	−100	0.0254
112	eukaryotic translation initiation factor 4H	G3HLP4	0.67 ± 0.23	0 ± 0	−100	0.0256
113	ferritin heavy chain	P29389	2.39 ± 0.27	0 ± 0	−100	0.0001
114	glutaredoxin-1	G3H756	0.55 ± 0.18	0 ± 0	−100	0.0243
115	heterogeneous nuclear ribonucleoprotein U	G3H7M8	0.93 ± 0.32	0 ± 0	−100	0.0271
116	histone H2B	A0A061IP52	6.48 ± 2.37	0 ± 0	−100	0.0338
117	histone H2B	G3H2T4	6.48 ± 2.37	0 ± 0	−100	0.0338
118	histone H2B	G3H2U0	6.48 ± 2.37	0 ± 0	−100	0.0338
119	histone H2B	G3HDU3	6.48 ± 2.37	0 ± 0	−100	0.0338

DOI: 10.1021/jf506118j
J. Agric. Food Chem. 2015, 63, 1869−1881

Table 1. continued

	protein name	protein ID	control (mean ± SE)	HF[a] (mean ± SE)	fold[b]	t-test p-value[c]
120	histone H2B	G3HPV1	6.48 ± 2.37	0 ± 0	−100	0.0338
121	histone H2B	G3INX0	6.48 ± 2.37	0 ± 0	−100	0.0338
122	isovaleryl-CoA dehydrogenase, mitochondrial	G3ICJ8	2.26 ± 0.52	0 ± 0	−100	0.0048
123	methionine-R-sulfoxide reductase B2, mitochondrial	G3H5C7	0.73 ± 0.24	0 ± 0	−100	0.0242
124	methylcrotonoyl-CoA carboxylase subunit α	A0A061IQ54	0.55 ± 0.18	0 ± 0	−100	0.0243
125	methylcrotonoyl-CoA carboxylase subunit α, mitochondrial	G3I7H8	0.55 ± 0.18	0 ± 0	−100	0.0243
126	phosphoserine aminotransferase	G3IKH9	1.22 ± 0.11	0 ± 0	−100	0.0001
127	protein disulfide-isomerase A3	G3H0U6	7.28 ± 0.48	0 ± 0	−100	0.0001
128	putative 2-oxoglutarate dehydrogenase E1 component DHKTD1, mitochondrial	G3GVP3	1.1 ± 0.15	0 ± 0	−100	0.0003
129	RNA helicase	Q8K5D5	0.79 ± 0.27	0 ± 0	−100	0.0257
130	splicing factor, proline-and glutamine-rich	G3H9U3	0.75 ± 0.25	0 ± 0	−100	0.0243
131	talin-2-like protein	A0A061I0N6	3.32 ± 0.43	0 ± 0	−100	0.0002
132	talin-2-like protein	A0A061I1X9	3.32 ± 0.43	0 ± 0	−100	0.0002
133	talin-2-like protein	A0A061I7B4	2.23 ± 0.79	0 ± 0	−100	0.0296
134	tubulin β-4 chain	G3HCL2	3.59 ± 0.57	0 ± 0	−100	0.0007
135	urocanate hydratase	G3GRZ9	0.68 ± 0.25	0 ± 0	−100	0.0331

[a]High-fat group. [b]High-fat group/control group. [c]Significant level =0.05.

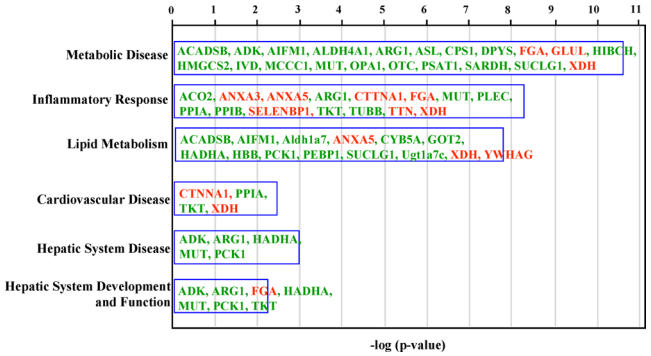

Figure 2. Proteins that were altered by the high-fat diet challenge and involved in metabolic diseases. Proteins marked green were down-regulated by the high-fat diet while those marked red were up-regulated. The full names of proteins are listed in Supporting Information Table 2. IPA computes a p score as $-\log_{10}(p\text{-value})$. A score of 3 or higher indicates that the proteins are not clustered in a pathway by random chance at the confidence level of 99.99% or higher.

perform the quantification of protein instead of two-dimensional electrophoresis (2-DE) as described in most studies.[16,29,30] Compared with 2-DE, label-free LC/MS/MS keeps the cost down and works more efficiently, allowing us to compare the expression of whole proteomics at a time. In addition to the changes in protein abundance, we also investigated the PTM of ANXA3, ANXA5, and XDH, three proteins that expressed differentially by the challenge of high-fat diet.

Body Weight and Organ Weight. Compared to control group, animals in high-fat group had lower daily feed intake; however, their weight gain, organ weight, and relative organ weight were higher than those of control group (Supporting Information Table 1).

Serum Lipids, AST, and ALT in Animals. Hamsters in the high-fat diet group had significantly ($p < 0.05$) higher serum TC and HDL-C (Supporting Information Figure 2). The level of serum TG was also higher in the high-fat group (Supporting Information Figure 2A), but not statistically significant ($p > 0.05$). The ratio of HDL-C to TC (Supporting Information Figure 2D) was lower in the high-fat group ($p > 0.05$). The activities of serum AST and ALT (Supporting Information Figure 2E and F), two clinical markers of liver damage, were significantly higher in animals maintained on the high-fat diet ($p < 0.05$).

Liver Lipids and Histopathology. Figure 1A shows the liver tissue of an animal in the control group while Figure 1B shows the liver tissue of an animal in the high-fat group. Microscopically, the liver from high-fat group revealed diffuse hepatocellular swelling with intracytoplasmic accumulation of lipid droplets (microvesicular steatosis). There were also multifocal, well-delineated ballooned hepatocytes in the periportal area. Some ballooned hepatocytes had pyknotic nuclei concurrent with varying degrees of neutrophils and lymphocytes infiltration.

Animals of high-fat group had significantly ($p < 0.05$) more hepatic TG and TC accumulation than those of control group (Figure 1C and E). Moreover, the average percentage of TG accumulated in the livers of high-fat group is higher than 5% (Figure 1D), which meets the clinical definition of fatty liver.[31]

Proteomic Analysis. Hepatic proteins were separated by electrophoresis and digested by trypsin before being analyzed by tandem mass spectrometry. The spectra generated were analyzed by TurboSequest to identify the peptide sequences against hamster database in UniProt. The results of analysis were scored using Xcorr. The proteins were regarded as hepatic proteins if more than two peptides from a single protein met the threshold of Xcorr score. On the basis of this criterion, 1191 proteins in liver were identified and 135 of them were altered by the challenge of high-fat diet (names of proteins and normalized spectrum counts of each protein were listed in Supporting Information Table 2). Table 1 shows the protein name, accession number, molecular function, and fold of change (high-fat/control) of all 135 proteins. Among these 135 proteins, 33 were up-regulated with the high-fat diet. The FDR (false discovery rate) of this analysis is 2.36%, higher than the minimal requirement of 5%. For some proteins that were not detected, it may result from their low abundance or the methodology of TurboSequest algorithm. By TurboSequest's specific algorithm, a protein will be ignored if it shares common sequences with other proteins that possess unique a peptide.

DOI: 10.1021/jf506118j
J. Agric. Food Chem. 2015, 63, 1869−1881

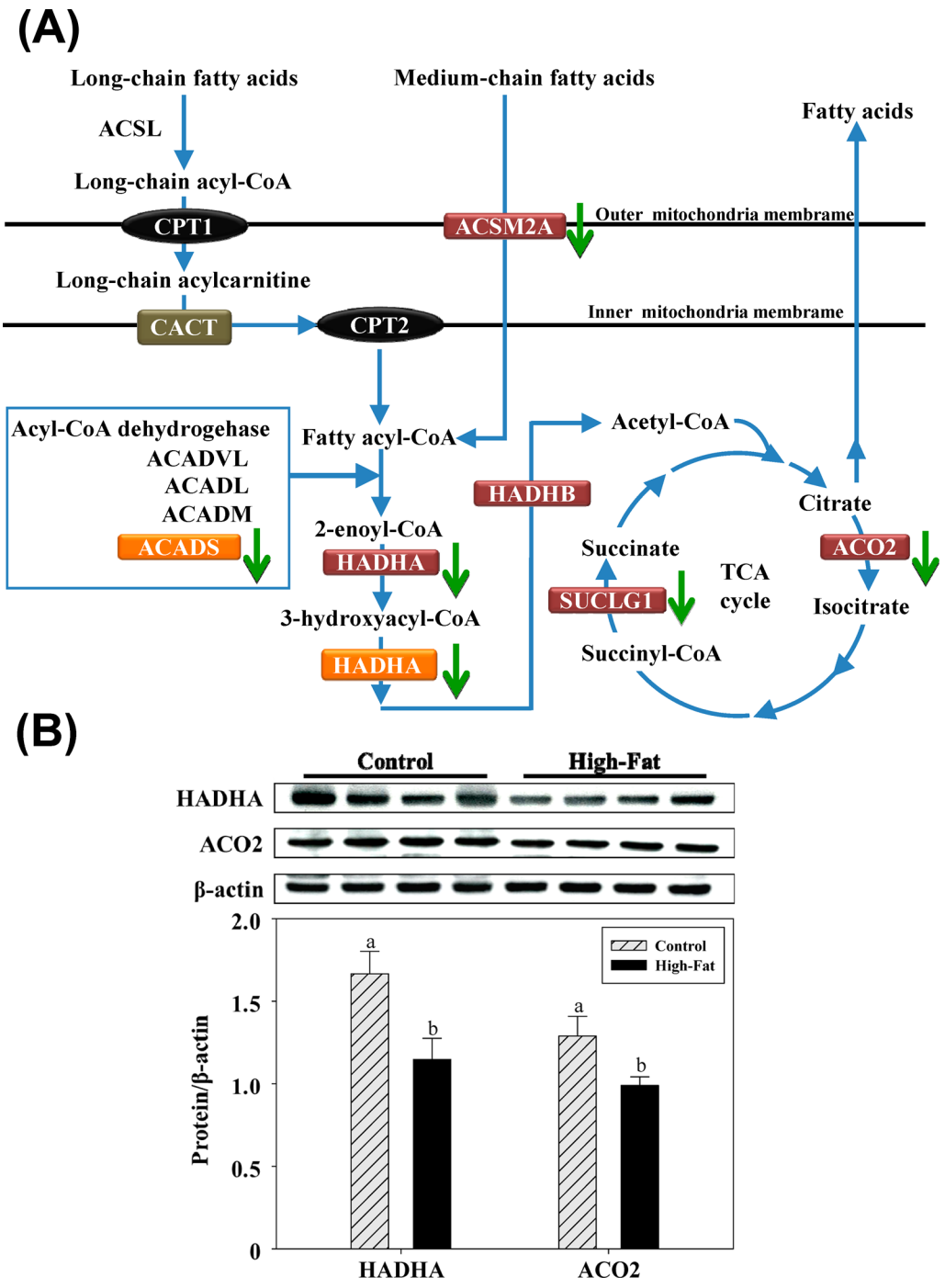

Figure 3. (A) Pathway of β-oxidation and TCA cycle. (B) Expression of HADHA and ACO2. Values are means of three replicated experiments. Groups with the same letter are not significantly different ($\alpha = 0.05$). Green arrows indicate down-regulation of proteins. ACSL, long-chain acyl-CoA synthase (ACSM refers to medium-chain acyl-CoA synthase); CPT, carnitine palmitoyltransferase; CACT, carnitine-acylcarnitine translocase; ACADS short-chain acyl-CoA dehydrogenase (VL, L, and M refer to very long-chain, long-chain, and medium-chain, respectively); HADHA, α-unit of mitochondrial trifunctional protein, containing the activities of enoyl-CoA hydratase and 3-hydroxyacyl-CoA dehydrogenase actvities; HADHB, β-unit of mitochondrial trifunctional protein, containing the activity of 3-ketoacyl-CoA thiolase. ACO2, aconitate hydratase 2; SUCLG, succinyl-CoA ligase.

Ingenuity Pathways Analysis. The proteins with altered expression were assessed through IPA. IPA calculates a p score as $-\log_{10}(p\text{-value})$ to rank networks. A score of 3 or higher indicates that the proteins are not clustered in a pathway by random chance at the confidence level of 99.99% or higher. Because high-fat diet significantly contributes to the etiology of metabolic diseases, proteins grouped into the related interactions by IPA are shown in Figure 2 (the full names of proteins are listed in Supporting Information Table 3). Proteins marked green were down-regulated by the high-fat diet, while those marked red were up-regulated. For proteins involved in metabolic diseases, 18 were down-regulated and 3 were up-regulated. For those that play a role in inflammatory response, 8 were down-regulated and 7 were up-regulated. With regard to

DOI: 10.1021/jf506118j
J. Agric. Food Chem. 2015, 63, 1869−1881

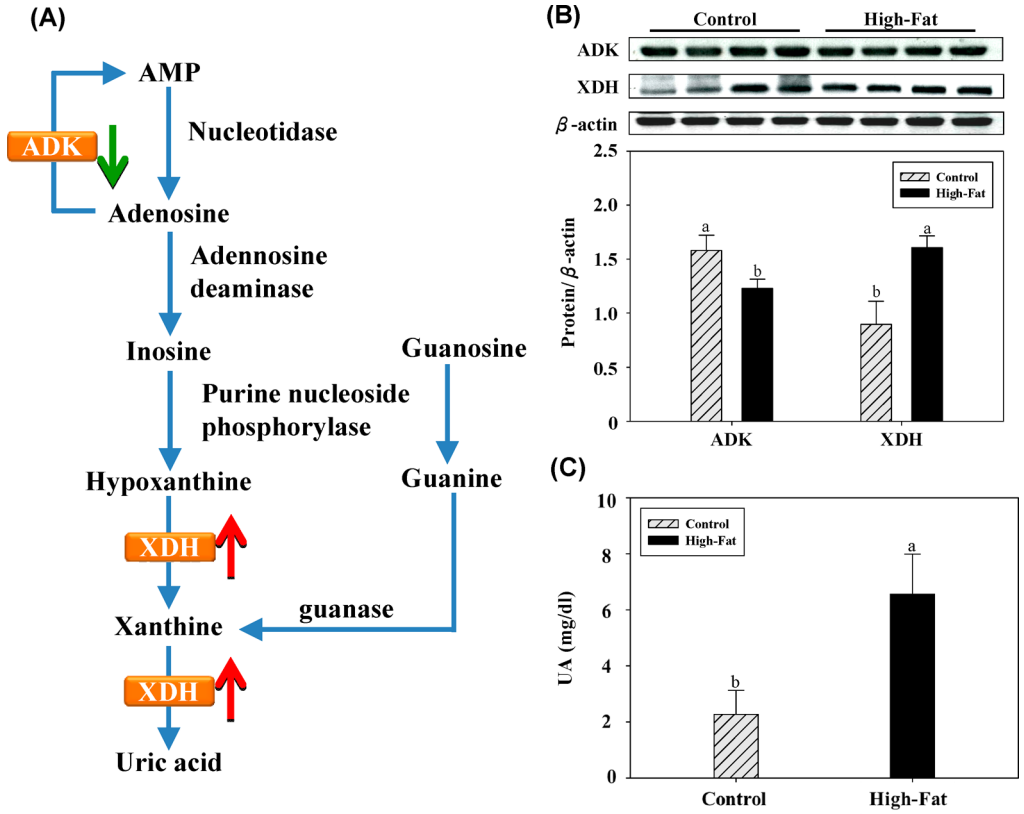

Figure 4. (A) Pathway of uric acid synthesis. (B) Expression of ADK and XDH. (C) Serum concentration of uric acid. Values are means of three replicated experiments. Groups with the same letter are not significantly different (α = 0.05). Green arrows indicate down-regulation of proteins and red arrows indicate up-regulation of proteins. ADK, adenosine kinase; XDH, xanthine dehydrogenase; UA, uric acid.

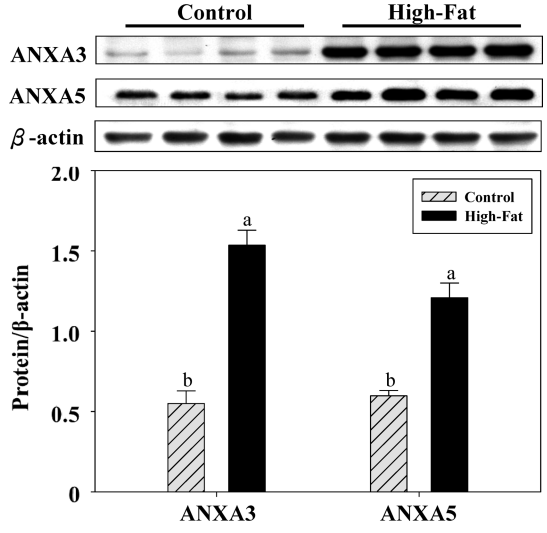

Figure 5. Expression of ANXA3 and ANXA5. Values are means of three replicated experiments. Groups with the same letter are not significantly different (α = 0.05). ANX, annexin.

lipid metabolism, 11 proteins were down-regulated and 3 were up-regulated. For proteins related to the development of cardiovascular disease, 2 were up-regulated and 2 were down-regulated. In the pathways involved in hepatic functions and diseases, 6 were down-regulated and 1 was up-regulated. Further Western blotting analysis was carried out to confirm the expression of some proteins mentioned above.

Expression of Enzymes Involved in Fatty Acid β-Oxidation. Mitochondrial β-oxidation is the main route for metabolism of fatty acids.[32] Prior to the translocation into mitochondria for β-oxidation, free long-chain fatty acids (LCFAs) must be activated by acyl-CoA synthetase long-chain (ACSL) (Figure 3A). After being activated to the CoA derivative, LCFAs translocate into a mitochondrion via the carnitine transacylation pathway, but medium-chain fatty acids can enter mitochondria without the carnitine shuttle. ACSs are classified as short-chain ACS (ACSS), medium-chain (ACSM), and ACSL according to their specificities for fatty acids of varying length.[33] Proteomic analysis shows that the expression of ACSM2A (medium-chain acyl-CoA synthetase family member 2A) was down-regulated by the high-fat diet (Table 1). Attenuated expression of ACSM2A decreased the opportunity for medium-chain fatty acids being transported into mitochondria for β-oxidation.

The first reaction within mitochondrial matrix is the acyl-CoA dehydrogenation catalyzed by acyl-CoA dehydrogenase (ACAD) (Figure 3A). Nine members were identified in the ACAD family, including the four members that are involved in β-oxidation: short, medium, long, and very long chain acyl-CoA dehydrogenase (ACADS, ACADM, ACADL, and ACADVL, respectively).[34] Following dehydrogenation, enoyl-CoA hydratase catalyzes the formation of 3-hydroxyacyl-CoA, which is further followed by the formation of 3-ketoacyl-CoA. Finally, acetyl-CoA is generated through a thiolysis reaction. The last three steps of reactions are catalyzed by mitochondrial trifunctional protein (MTP), which is composed of an α-unit (HADHA) and a β-unit (HADHB). HADHA contains long-chain enoyl-CoA hydratase and 3-hydroxyacyl-CoA dehydro-

DOI: 10.1021/jf506118j
J. Agric. Food Chem. 2015, 63, 1869−1881

Table 2. Post-translational Modifications of ANXA3, ANXA5, and XDH

protein	PTM	site	modified peptides	position[a]	obs. m/z[b]	calc. m/z[c]	dM[d]
ANXA3[e]	Hex-HexNac[g]	Thr (154)	ALL**T**$_{\#}$LADGRRDESLK	151−165	675.008	675.024	−0.016
	levuglandinyl-lysine lactam aduct[g]	Lys (93)	DDLKGDLSGHFEHIMVALVTAPALFDAK#	66−93	1114.919	1114.914	0.005
	n-octanoate[g]	Thr (303)	HYGYSLHSAIQSD**T**$_{\#}$SGDYRLVLLK	290−313	950.498	950.500	−0.002
ANXA5	NeuAc-Hex-Hex-HexNAc-Hex-HexNAc-Hex	Ser (116)	GAGTNEKVLTEIIAS#R	102−117	948.809	948.812	−0.003
	4-hydroxy-2-nonenal[g]	Lys (63)	TLFG**K**$_{\#}$DLLDDLK	59−70	505.946	505.959	−0.013
	4-hydroxynonenal[g]	Lys (301)	KNFATSLYSMI**K**$_{\#}$GDTSGDYK	290−309	794.743	794.733	0.01
	NE-(carboxymethyl)lysine[g]	Lys (76)	TLFGKDLLDDLKSELTG**K**$_{\#}$	59−76	684.361	684.367	−0.006
	carboxylation[g]	Glu (107)	GAGTN**E**$_{\#}$KVLTEIIASR	102−117	851.948	851.951	−0.003
	oxoalanine[g]	Ser (44)	GLGTDEESILTLLT**S**$_{\#}$R	30−45	851.948	851.946	0.002
XDH[f]	carboxylation	Glu (231)	FEG**E**$_{\#}$RVTWIQASTLGELLDIKAQHPDAK	228−255	1066.216	1066.213	0.003
	4-oxo-2-nonenal	Lys (890)	SIMERALFHMDNAY**K**$_{\#}$	876−890	654.665	654.657	0.008
	dihydroxylation	Lys (270)	AQHPDAKLVVGNTEIGIEM*KF**K**$_{\#}$	249−270	825.096	825.094	0.002
	S-farnesyl cysteine[g]	Cys (112)	SHGSQ**C**$_{\#}$GFCTPGIVM*SM*YTLLR	107−128	910.447	910.446	0.001
	methylation[g]	His (884)	ALF**H**$_{\#}$MDNAY**K**$_{\#}$IPNI**R**$_{\#}$	881−895	923.009	922.993	0.016
		Lys (890)					
		Arg (895)					
	monoglutamyl[g]	Glu (960)	LE$_{\#}$VFNLPR	959−966	558.824	558.805	0.019

[a]Site of modified peptide. [b]Obs.: observed m/z of the modified peptides. [c]Calc.: calculated m/z of the modified peptides. [d]The difference between obs. and calc. [e]ANX: annexin. [f]XDH: xanthine dehydrogenase. [g]Presence in high-fat group.

genase actvities, whereas HADHB contains the 3-ketoacyl-CoA thiolase activity.[35]

Proteomic analysis shows that the expression of ACADS and HADHA was down-regulated by the high-fat diet challenge (Table 1 and Figure 3B). Down-regulation of ACAD and HADHA would limit the capacity of mitochondria to oxidize fatty acids, leading to hepatic steatosis. Mice deficient in short-chain ACAD (ACADS) develop a fatty liver upon dietary fat challenge.[36] Medium-chain acyl-CoA dehydrogenase (ACADM) is the most common inherited disorder of mitochondrial β-oxidation in humans. Mice deficient in ACADM also develop a fatty liver.[37] MTP consists of four α and four β subunits that catalyze the final three steps of long-chain fatty acid β-oxidation. Newborn mice with MTP α subunit (HADHA) null allele ($Mtpa^{-}/^{-}$) revealed rapid development of hepatic steatosis after birth and significant necrosis of cardiac myocytes later.[35] In the aging heterozygous $Mtpa^{+}/^{-}$ mice, significantly higher hepatic triglyceride content and serum ALT activity were measured compared with the $Mtpa^{+}/^{+}$ littermates.[38] Rats with a high-fat diet induced hepatic steatosis had reduced level of enoyl-coenzyme A hydratase. Down-regulation of enoyl-coenzyme A hydratase in mice significantly exacerbated high-fat diet induced hepatic steatosis.[16]

In this study, decreased expression of ACSM2A, ACADS, and HADHA in the high-fat group (Table 1 and Figure 3B) may attenuate the oxidation of fatty acids, increasing the availability of fatty acids for synthesis of TG. This finding may explain the development of fatty liver as observed in the high-fat group.

Expression of Enzymes Involved in TCA Cycle. Acetyl-CoA enters TCA cycle by condensing with oxaloacetate to form citrate (Figure 3A). The citrate is then converted to isocitrate through the action of aconitate hydratase (ACO, also named as aconitase). Isocitrate undergoes dehydrogenation and decarboxylation to form α-ketoglutarate. Ketoglutarate is further decarboxylated to form succinyl-CoA. To continue the cycle, succinyl-CoA is converted to succinate by the action of succinyl-CoA ligase (also called succinate synthetase or succinate thiokinase). Succinate is further metabolized to fumurate, followed by the formation of malate. Malate is then converted to oxaloacetate through dehydrogenation reaction.[39]

Proteomic analysis showed the ACO was down-regulated by high-fat diet (Table 1 and Figure 3B). Mammals express two isoforms of ACO, ACO1 (soluble), and ACO2 (mitochondrial). Cui et al. found a significant decrease of ACO2 expression in splenic lymphocytes of mice that were fed a high-fat diet for 10 weeks.[40] Loss of ACO activity limits TCA cycle activity, which will favor the translocation of citrate from mitochondria to cytosol to undergo fatty acid synthesis.[41]

Proteomic analysis showed that SUCLG1 was also down-regulated by high-fat diet (Table 1). SUCLG converts succinyl-CoA to succinate and free coenzyme A, and converts adenosine diphosphate (ADP) to adenosine triphosphate (ATP) or guanosine diphosphate (GDP) to guanosine triphosphate (GTP). SUCLG is composed of two subunits, and the α-subunit is encoded by *SUCLG1* gene with specificity for GDP. Liver biopsy of subjects with SUCLG1 deficiency showed both micro- and macrosteatosis.[42]

Expression of Enzymes Involved in Uric Acid Synthesis. Uric acid is the final breakdown product of purine metabolism. In the metabolism of purine nucleotide, adenosine is first deaminated to inosine in the reaction catalyzed by deaminase or phosphorylated to AMP by the action of adenosine kinase (ADK) (Figure 4A).[43] Catalyzed by purine nucleotide phosphorylase, inosine and guanosine are converted to hypoxanthine and guanine, respectively. Hypoxanthine and guanine next form xanthine in reactions catalyzed by xanthine dehydrogenase (XDH) and guanase, respectively. Xanthine is then oxidized to uric acid by the second reaction catalyzed by XDH.[44]

In the present study, the high-fat diet down-regulated ADK but up-regulated XDH (Table 1 and Figure 4B). ADK is highly expressed in liver. It is essential for maintaining normal level of adenine nucleotides and S-adenosylmethionine-dependent transmethylation process.[43] A decreased level of ADK decreases the recycle of adenosine to AMP, leading to more adenosine available for the biosynthesis of uric acid and reduced level of

DOI: 10.1021/jf506118j
J. Agric. Food Chem. 2015, 63, 1869−1881

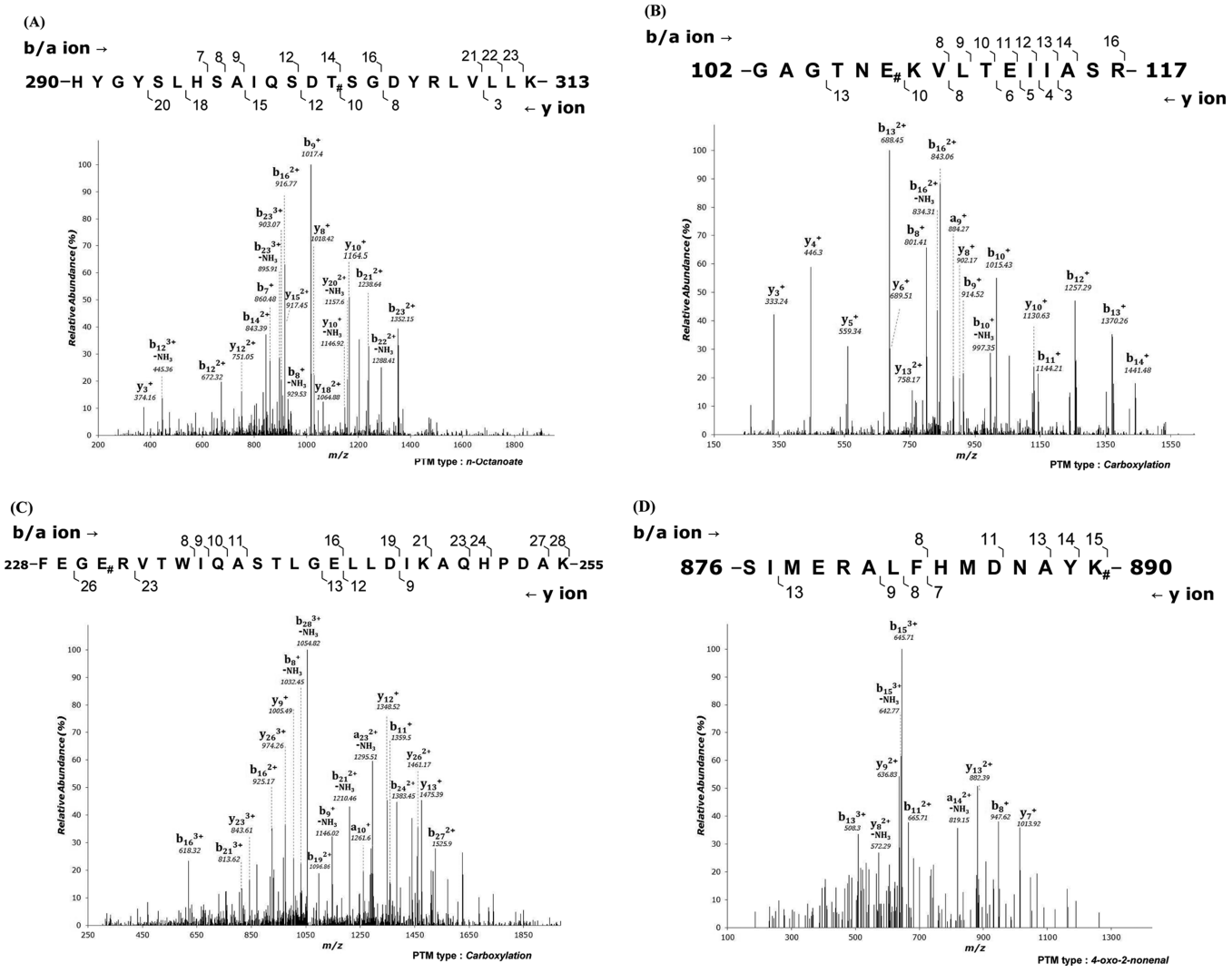

Figure 6. (A) Tandom mass spectrum of the *n*-octanoate peptide with the sequence 290-HYGYSLHSAIQSDT$_{\#}$SGDYRLVLLK-313 on ANXA3. (B) Tandom mass spectrum of the carboxylation peptide with the sequence 102-GAGTNEKVLTEIIAS#R-117 on ANXA5. (C) Tandom mass spectrum of the carboxylation peptide with the sequence 228-FEGE$_{\#}$RVTWIQASTLGELLDIKAQHPDAK-255 on XDH. (D) Tandom mass spectrum of the 4-oxo-2-nonenal peptide with the sequence 876-SIMERALFHMDNAYK$_{\#}$-890 on XDH. ANX, annexin; XDH, xanthine dehydrogena.

adenine nucleotides. Because the metabolic rate in liver mitochondria is proportional to the level of adenine nucleotides, a decreased amount of adenine nucleotides in the liver would lead to an impairment of mitochondrial function. Newborns with *Adk*$^{-/-}$ displayed microvesicular hepatic steatosis and died within 14 days with fatty livers.[44]

Xanthine oxidoreductase, a member of molybdoenzyme family, has two interconvertible forms, xanthine dehydroenase (XDH) and xanthine oxidase (XO). Both XDH and XO catalyze the conversion of hypoxanthine to xanthine and xanthine to uric acid.[45] Under physiological conditions, the enzyme is primarily present as XDH. Up-regulated expression of XDH by the challenge of a high-fat diet in the current study (Figure 4B) promoted the formation of uric acid, as indicated by the increased serum concentration of uric acid in animals of high-fat group (Figure 4C). Because high uric acid levels may cause frequent attacks of gout, it is reasonable to infer that high-fat diet is associated with etiology of gout.

Expression of Annexin A3 and Annexin A5. In this present study, proteomic analysis indicated that the challenge of a high-fat diet up-regulated both annexin A3 (ANXA3) and annexin A5 (ANXA5) (Table 1 and Figure 5). ANXs are a family of Ca^{2+}-regulated membrane- and phospholipid-binding proteins that have been implicated in many cellular processes including inflammation, apoptosis, proliferation, and differentiation.[46] Annexin A3 is a novel angiogenic factor that induces vascular endothelial growth factor (VEGF) production through the hypoxia-inducible factor-1 (HIF-1) pathway.[47] Poloxamer P-407 hyperlipidemia mouse is a nondiet-induced and genetically unaltered model of atherosclerosis. Kuzman et al. detected an up-regulation of annexin A3 in this mouse model.[48] By using an experimental model of tumor necrosis factor-α (TNF-α)-mediated inflammation, Pitroda et al. reported increased expression of ANXA3 in four types of human cancer and several human diseases associated with chronic inflammation.[49]

ANXA5 is associated with the development and progression of breast cancer, prostate cancer, cervical cancer, colorectal adenocarcinoma, gastric cancer, pancreatic adenocarcinoma, sarcoma, bladder cancer, and glioma. ANXA5 is considered as a predictive marker for tumor development and a therapeutic target for early diagnosis and treatment of tumors.[50] In the

DOI: 10.1021/jf506118j
J. Agric. Food Chem. 2015, 63, 1869–1881

present study, up-regulation of ANXA3 and ANXA5 implies an inflammatory and procarcinogenic status induced by high-fat diet.

Expression of Enzymes Involved in Urea Synthesis. The urea cycle is the major pathway for detoxification of ammonia in mammals. In the present study, proteomic analysis showed that several enzymes involved in urea synthesis were down-regulated by high-fat diet, including carbamoyl-phosphate synthetase 1 (CPS1), ornithine transcarbamoylase (OTC), argininosuccinate synthetase (ASS), argininosuccinate lyase (ASL), and arginase 1 (ARG1) (Table 1 and Supporting Information Figure 3).

CPS1 and OTC are mitochondrial enzymes catalyzing the first and second steps of the urea cycle, respectively. The expression of both enzymes is higher in hepatocytes than in other tissues.[51] Deficiency and reduced activity of CPS1/OTC cause hyperammonaemia.[52,53] ASS catalyzes the reversible condensation of citrulline with aspartate to form argininosuccinate. Argininosuccinate is then split into arginine and funarate in a reaction catalyzed by ASL. ASS is a highly conserved enzymes expressed in various tissues. Decreased expression of ASS attenuates the metabolism of ammonia and formation of argininosuccinate, resulting in abnormally higher concentration of ammonia and citrulline in the blood.[54] Patients with ASL deficiency were detected with increased blood ammonia.[55] ARG is the final enzyme of the urea cycle, catalyzing the metabolism of arginine to urea and ornithine. ARG1 knockout mice exhibited severe symptoms of hyperammonemia and hepatocyte abnormalities.[56,57]

Post-translational Modification of ANXA and XDH. PTMs are site specific amino acid side chain alterations taking place after translation of mRNA into a protein. It affects the folding, conformation, and functions of proteins. More than 300 different types of PTMs have been characterized to date, including carboxylation, methylation, phosphorylation, glycosylation, carboxylation, ubiquitination, prenylation, and sulphation. PTMs lead to higher structural and functional protein diversity, playing significant roles in physiological process and disease progression.[58,59] Identification of PTM on ANXA3, ANXA5, and XDH were carried out by our in-house PTM finder programs PTM-Miner and PTM-Q. The identified peptides and corresponding modified sites are listed in Table 2.

Four representative spectra for ANXA3, ANXA5, and XDH are shown in Figure 6. Figure 6A is the fragment ion spectrum for the modified peptide 290-HYGYSLH-SAIQSD**T**$_{\#}$SGDYRLVLLK-313 of ANXA3. The spacing of b and y ions was used to decipher the sequence of modified peptide. The novel *n*-octanoate site was detected based on the unmodified b14 ion and the mass shift of 126.10 Da for the y12 ion on modified peptide. The matched peaks were labeled according to the Biemann nomenclature. Figure 6B shows the fragment ion spectrum for the modified peptide 102-GAGTN**E**$_{\#}$KVLTEIIASR-117 of ANXA5. The novel carboxylation site was detected based on the unmodified y10 ion and the mass shift of 43.99 Da for the b8 ion on modified peptide. Figure 6C is the fragment ion spectrum for the modified peptide 228-FEG**E**$_{\#}$RVTWIQASTLGELLDIKAQHPDAK-255 of XDH. The novel carboxylation site was detected based on the unmodified y23 ion and the mass shift of 43.99 Da for the b8 ion on modified peptide. Figure 6D shows the fragment ion spectrum for the modified peptide 876- SIMERALFHMD-NAY**K**$_{\#}$-890 of XDH. The novel 4-oxo-2-nonenal site was detected based on the unmodified b14 ion and the mass shift of 136.09 Da for the y7 ion on modified peptide.

Proteomics is a powerful tool in monitoring the changes of protein profile induced by dietary manipulation. The findings of this study show that the challenge of a high-fat diet for 8 weeks impairs β-oxidation and ammonia metabolism; moreover, the high-fat diet up-regulates expression of inflammatory markers and synthesis of uric acid.

■ ASSOCIATED CONTENT

Ⓢ Supporting Information

Supporting tables and figures. This material is available free of charge via the Internet at http://pubs.acs.org.

■ AUTHOR INFORMATION

Corresponding Author

*E-mail: drkuo@mail.usc.edu.tw. Tel: 886-2-25381111-6214.

Funding

This study was supported by National Scientific Council, Taiwan (NSC 101-2313-B-158-001) and Shih Chien University (USC-101-05-02001).

Notes

The authors declare no competing financial interest.

■ REFERENCES

(1) Eckel, R. H.; Grudy, G. M.; Zimmet, P. Z. The metabolic syndrome. *Lancet* **2005**, *365*, 1415−1428.

(2) Matteoni, C. A.; Younossi, Z. M.; ramlich, T.; Boparai, N.; Liu, Y. C.; Mccullough, A. J. Nonalcoholic fatty liver disease: A spectrum of clinical and pathological severity. *Gastroenterology* **1999**, *116*, 1413−1419.

(3) Angulo, P.; Lindor, K. D. Treatment of nonalcoholic steatohepatitis. *Best Pract. Res. Clin. Gastroenterol.* **2002**, *16*, 797−810.

(4) Memon, R. A.; Feingold, K. R.; Moser, A. H.; Fuller, J.; Grundeld, C. Regulation of fatty acid transport protein and fatty acid translocase mRNA levels by endotoxin and cytokines. *Am. J. Physiol.* **1998**, *274*, E210−E217.

(5) Ryedn, M.; Dicker, A.; van Harmelen, V.; Hauner, H.; Brunnberg, M.; Perbeck, L.; Lonnqvist, F.; Arner, P. Mapping of early signaling events in tumor necrosis factor-α-mediated lipolysis in human fat cells. *J. Biol. Chem.* **2002**, *277*, 1085−1091.

(6) Bradbury, M. W.; Berk, P. D. Lipid metabolism in hepatic steatosis. *Clin. Liver Dis.* **2004**, *8*, 639−671.

(7) Dentin, R.; Girard, J.; Postic, C. Carbohydrate responsive element binding protein (ChREBP) and sterol regulatory element binding protein-1c (SREBP-1c): Two key regulators of glucose metabolism and lipid synthesis in liver. *Biochimie* **2005**, *87*, 81−86.

(8) Anderson, N. L.; Anderson, N. G. Proteome and proteomics: New technologies, new concepts, and new words. *Electrophoresis* **1998**, *19*, 1853−1861.

(9) Morand, J. P.; Macri, J.; Adeli, K. Proteomics profiling of hepatic endoplasmic reticulum-associated proteins in an animal model of insulin resistance and metabolic dyslipidemia. *J. Biol. Chem.* **2005**, *280*, 17626−17633.

(10) Meneses-Lorente, G.; Watt, A.; Salim, K.; Gaskell, S. J.; Muniappa, N.; Lawrence, J.; Guest, P. C. Identification of early proteomic markers for hepatic steatosis. *Chem. Res. Toxicol.* **2006**, *19*, 986−989.

(11) Santamaria, E.; Muñoz, J.; Fernández-Irigoyen, J.; Prieto, J.; Corrales, F. J. Toward the discovery of new biomarkers of hepatocellular carcinoma by proteomics. *Liver Int.* **2007**, *27*, 163−173.

(12) Walther, T. C.; Mann, M. Mass spectrometry-based proteomics in cell biology. *J. Cell Biol.* **2010**, *190*, 491−500.

(13) Aldred, S.; Grant, M. M.; Griffiths, H. R. The use of proteomics for the assessment of clinical samples in research. *Clin. Biochem.* **2004**, *37*, 93−952.

DOI: 10.1021/jf506118j
J. Agric. Food Chem. 2015, 63, 1869−1881

(14) Marcotte, E. M. How do shotgun proteomics algorithms identify proteins? *Nat. Biotechnol.* **2007**, *25*, 755−757.
(15) Abdallah, C.; Dumas-Gaudot, E.; Renaut, J.; Slergeant, K. Gel-based and gel-free quantitative proteomics approaches at a glance. *Int. J. Plant Genomics* **2012**, *2012*, No. 494572.
(16) Zhang, X.; Yang, J.; Guo, Y.; Yu, C.; Xu, C.; Xu, L.; Wu, S.; Sun, W.; Wei, H.; Gao, X.; Zhu, Y.; Qian, X.; Jiang, Y.; Li, Y.; He, F. Functional proteomic analysis of nonalcoholic fatty liver disease in rat models: Enoyl-coenzyme A hydratase down-regulation exacerbates hepatic steatosis. *Hepatology* **2010**, *51*, 1190−1199.
(17) Baiges, I.; Palmfeldt, J.; Bladé, C.; Gregersen, N.; Arola, L. Lipogenesis is decreased by grape seed proanthocyanidins according to liver proteomics of rats fed a high fat diet. *Mol. Cell. Proteomics* **2010**, *9*, 1499−1513.
(18) Luo, M.; Mengos, A. E.; Stubblefield, T. M.; Mandarino, L. J. High fat diet-induced changes in hepatic protein abundance in mice. *J. Proteomics Bioinform.* **2012**, *5*, 60−66.
(19) Bertram, H. C.; Larsen, L. B.; Chen, X.; Jeppesen, P. B. Impact of high-fat and high-carbohydrate diets on liver metabolism studied in a rat model with a systems biology approach. *J. Agric. Food Chem.* **2012**, *60*, 676−684.
(20) Bhathena, J.; Kulamarva, A.; Martoni, C.; Urbanska, A. M.; Malhotra, M.; Paul, A.; Prakash, S. Diet-induced metabolic hamster model of nonalcoholic fatty liver disease. *Diabetes Metab. Syndr. Obes. Target Ther.* **2011**, *4*, 195−203.
(21) Folch, J.; Lees, M.; Sloane Stanley, G. H. A simple method for the isolation and purification of total lipids from animal tissues. *J. Biol. Chem.* **1957**, *226*, 497−509.
(22) Liao, C. C.; Chen, Y. W.; Jeng, T. L.; Li, C. R.; Kuo, C. F. Consumption of purple sweet potato affects post-translational modification of plasma proteins in hamsters. *J. Agric. Food Chem.* **2013**, *61*, 12450−12458.
(23) Rajkumar, R.; Karthikeyan, K.; Archunan, G.; Huang, P. H.; Chen, Y. W.; Ng, W. V.; Liao, C. C. Using mass spectrometry to detect buffalo salivary odorant-binding protein and its post-translational modifications. *Rapid Commun. Mass Spectrom.* **2010**, *24*, 3248−54.
(24) Lundgren, D. H.; Han, D. K.; Eng, J. K. Protein identification using TurboSEQUEST. *Curr. Protoc. Bioinformatics* **2005**, *10*, 13.3.1−13.3.13.
(25) Piersma, S. R.; Fiedler, U.; Span, S.; Lingnau, A.; Pham, T. V.; Hoffmann, S.; Kubbutat, M. H.; Jiménez, C. R. Workflow comparison for label-free, quantitative secretome proteomics for cancer biomarker discovery: Method evaluation, differential analysis, and verification in serum. *J. Proteome Res.* **2010**, *9*, 1913−1922.
(26) Uen, Y.-H.; Lin, K.-Y.; Sun, D.-P.; Liao, C.-C.; Hsieh, M.-S.; Huang, Y.-K.; Chen, Y.-W.; Huang, P.-H.; Chen, W.-J.; Tai, C.-C.; Lee, K.-W.; Chen, Y.-C.; Lin, C.-Y. Comparative proteomics, network analysis, and post-translational modification identification reveal differential profiles of plasma Con A-bound glycoprotein biomarkers in gastric cancer. *J. Proteomics* **2013**, *83*, 197−213.
(27) Stein, O.; Thiery, J.; Stein, Y. Is there a genetic basis for resistance to atherosclerosis. *Atherosclerosis* **2002**, *160*, 1−10.
(28) Zhang, Z.; Wang, H.; Jiao, R.; Peng, C.; Wong, Y. M.; Yeung, V. S. Y.; Huang, Y.; Chen, Z.-Y. Choosing hamsters but not rats as a model for studying plasma cholesterol-lowering activity of functional foods. *Mol. Nutr. Food Res.* **2009**, *53*, 921−930.
(29) Zhang, L.; Perdomo, G.; Kim, D. H.; Qu, S.; Ringquist, S.; Trucco, M.; Dong, H. Proteomic analysis of fructose-induced fatty liver in hamsters. *Metabolism* **2008**, *57*, 1115−1124.
(30) Li, Lin.; Lu, D.-Z.; Li, Y.-M.; Zhang, X.-Q.; Zhou, X.-X.; Jin, X. Proteomic analysis of liver mitochondria from rats with nonalcoholic steatohepatitis. *World J. Gastroenterol.* **2014**, *20*, 4778−4786.
(31) Hernaez, R.; Lazo, M.; Bonekamp, S.; Kamel, I.; Brancati, F. L.; Guallar, E.; Clark, J. M. Diagnostic accuracy and reliability of ultrasonography for the detection of fatty liver: A meta-analysis. *Hepatology* **2011**, *54*, 1082−1090.
(32) Reddy, J. K. Nonalcoholic steatosis and steatohepatitis. III. Peroxisomal β-oxidation, PPAR α, and steatohepatitis. *Am. J. Physiol. Gastrointest. Liver Physiol.* **2001**, *281*, G1333−G1339.
(33) Watkins, P. Fatty acid activation. *Prog. Lipid Res.* **1997**, *36*, 55−83.
(34) Kim, J.-J.; Miura, R. Acyl-CoA dehydrogenases and acyl-CoA oxidases, structural basis for mechanistic similarities and differences. *Eur. J. Biochem.* **2004**, *271*, 483−493.
(35) Ibdah, J. A.; Paul, H.; Zhao, Y.; Binford, S.; Salleng, K.; Cline, M.; Matern, D.; Bennett, M. J.; Rinaldo, P.; Strauss, A. W. Lack of mitochondrial trifunctional protein in mice causes neonatal hypoglycemia and sudden death. *J. Clin. Invest.* **2001**, *107*, 1403−1409.
(36) Wood, P. A.; Amendt, B. A.; Rhead, W. J.; Millington, D. S.; Inoue, F.; Armstrong, D. Short-chain acyl-coenzyme A dehydrogenase deficiency in mice. *Pediatr. Res.* **1989**, *25*, 38−43.
(37) Tolwani, R. J.; Hamm, D. A.; Tian, L.; Sharer, J. D.; Vockley, J.; Rinaldo, P.; Matern, D.; Schoeb, T. R.; Wood, P. A. Medium-chain acyl-CoA dehydrogenase deficiency in gene-targeted mice. *PloS Genet.* **2005**, *1*, 205−212.
(38) Ibdah, J. A.; Perlegas, P.; Zhao, E.; Angdisen, J.; Borgerink, H.; Shadoan, M. K.; Wagner, J. D.; Matern, D.; Rinaldo, P.; Cline, J. M. Mice heterozygous for a defect in mitochondrial trifunctional protein develop hepatic steatosis and insulin resistance. *Gastroenterology* **2005**, *128*, 1381−1390.
(39) Krebs, H. A. Rate control of the tricarboxylic acid cycle. *Adv. Enzyme Regul.* **1970**, *8*, 335−353.
(40) Cui, J.; Xiao, Y.; Shi, Y.-H.; Le, G. W.; Miao, X. Y. Comparative proteome analysis of splenic lymphocytes in long-term high-fat diet and dietary supplement with lipoic acid mice. *Cell. Immunol.* **2010**, *264*, 156−162.
(41) Hanson, R. W.; Ballard, F. J. The relative significance of acetate and glucose as precursors for lipid synthesis in liver and adipose tissue from ruminants. *Biochem. J.* **1967**, *105*, 529−536.
(42) Van Hove, J. L. K.; Saenz, M. S.; Thomas, J. A.; Gallaghe, R.; Lovell, M. A.; Fenton, L. Z.; Shanske, S.; Myers, S. M.; Wanders, R. J. A.; Ruiter, J.; Turkenburg, M.; Waterham, H. R. Succinyl-CoA ligase deficiency: A mitochondrial hepatoencephalomyopathy. *Pediatr. Res.* **2010**, *68*, 159−164.
(43) Bjursell, M. K.; Blom, H. J.; Cayuela, J. A.; Engvall, M. L.; Lesko, N.; Balasubramaniam, S.; Brandberg, G.; Halldin, M.; Falkenberg, M.; Jakobs, C.; Smith, D.; Struys, E.; Döbeln, U.; Gustafsson, C. M.; Lundeberg, J.; Wedell, A. Adenosine kinase deficiency disrupts the methionine cycle and causes hypermethioninemia, encephalopathy, and abnormal liver function. *Am. J. Hum. Genet.* **2011**, *89*, 507−511.
(44) Boison, D.; Scheurer, L.; Zumsteg, V.; Rülicke, T.; Litynski, P.; Fowler, B.; Brandner, S.; Mohler, H. Neonatal hepatic steatosis by disruption of the adenosine kinase gene. *Proc. Natl. Acad. Sci., U.S.A.* **2002**, *99*, 6985−6990.
(45) Hille, R.; Nishino, T. Xanthine oxidase and xanthine dehydrogenase. *FASEB J.* **1995**, *9*, 995−1003.
(46) Gerke, V.; Moss, S. E. Annexins: From structure to function. *Physiol. Rev.* **2002**, *82*, 331−371.
(47) Park, J. E.; Lee, D. H.; Lee, J. A.; Park, S. G.; Kim, N.-S.; Park, B.-C.; Cho, S. Annexin A3 is a potential angiogenic mediator. *Biochem. Biophys. Res. Commun.* **2005**, *337*, 1283−1287.
(48) Kuaman, D.; Tacer, K. F.; Cerne, M.; Rezen, T.; Acimovic, J.; Cegovnik, U.; Kocjan, D.; Urleb, U.; Rozman, D. Modulation of hepatic transcriptome in the poloxamer P-407 hyperlipidemia mouse model. *Acta Chim. Stov.* **2009**, *56*, 262−269.
(49) Pitroda, S. P.; Zhou, T.; Sweis, R. F.; Filippo, M.; Labay, E.; Beckett, M. A.; Mauceri, H. J.; Liang, H.; Darga, T. E.; Perakis, S.; Khan, S. A.; Sutton, H. G.; Zhang, W.; Khodarev, N. N.; Garcia, J. G. N.; Weichselbaum, R. R. Tumor endothelial inflammation predicts clinical outcome in diverse human cancers. *PloS One* **2012**, *7*, e46104.
(50) Peng, B.; Guo, C.; Guan, H.; Liu, S.; Sun, M.-Z. Annexin A5 as a potential marker in tumors. *Clin. Chim. Acta* **2014**, *427*, 42−48.
(51) Ryall, J.; Nguyen, M.; Bendayan, M.; Shore, G. C. Expression of nuclear genes encoding the urea cycle enzymes, carbamoyl-phosphate synthetase I and ornithine carbamoyl transferase, in rat liver and intestinal mucosa. *Eur. J. Biochem.* **1985**, *152*, 287−292.

DOI: 10.1021/jf506118j
J. Agric. Food Chem. 2015, 63, 1869−1881

(52) Nakamura, K.; Kido, J.; Mitsubuchi, H.; Endo, F. Diagnosis and treatment of urea cycle disorders in Japan. *Pediatr. Int.* **2014**, *56*, 506−509.
(53) Ihara, K.; Miyako, K.; Ishimura, M.; Kuromaru, R.; Wang, H. Y.; Yasuda, K.; Hara, T. A case of hyperinsulinism/hyperammonaemia syndrome with reduced carbamoyl-phosphate synthetase-1 activity in liver: A pitfall in enzymatic diagnosis for hyperammonaemia. *J. Inherit. Metab. Dis.* **2005**, *28*, 681−687.
(54) Husson, A.; Brasse-Lagnel, C.; Fairand, A.; Renouf, S.; Lavoinne, A. Argininosuccinate synthetase from the urea cycle to the citrulline−NO cycle. *Eur. J. Biochem.* **2003**, *270*, 1887−1899.
(55) Ficicioglu, C.; Mandell, R.; Shih, V. E. Argininosuccinate lyase deficiency: Long term outcome of 13 patients detected by newborn screening. *Mol. Genet. Metab.* **2009**, *98*, 273−277.
(56) Iyer, R. K.; Jenkinson, C. P.; Vockley, J. G.; Kern, R. M.; Grody, W. W.; Cederbaum, S. D. The human arginases and arginase deficiency. *J. Inherit. Metab. Dis.* **1998**, *1* (suppl. 21), 86−100.
(57) Iyer, R. K.; Yoo, P. K.; Kern, R. M.; Rozengurt, N.; Tsoa, R.; O'Brien, W. E.; Yu, H.; Grody, W. W.; Cederbaum, S. D. Mouse model for human arginase deficiency. *Mol. Cell. Biol.* **2002**, *22*, 4491−4498.
(58) Witze, E. S.; Old, W. M.; Resing, K. A.; Ahn, N. G. Mapping protein post-translational modifications with mass spectrometry. *Nat. Methods* **2007**, *4*, 798−806.
(59) van Kasteren, S. I.; Kramer, H. B.; Jensen, H. H.; Campbell, S. J.; Kirkpatrick, J.; Oldham, N. J.; Anthony, D. C.; Davis, B. G. Expanding the diversity of chemical protein modification allows post-translational mimicry. *Nature* **2007**, *446*, 1105−1109.

DOI: 10.1021/jf506118j
J. Agric. Food Chem. 2015, 63, 1869−1881